Influence of hydrogenation conditions on the structural, optical, and magnetic properties of degenerated Ni/Al co-doped anatase nanocomposite

A. A. Dakhel (✉ adakhil@uob.edu.bh)

University of Bahrain

Influence of hydrogenation conditions on the structural, optical, and magnetic properties of degenerated Ni/Al co-doped anatase nanocomposite

A. A. Dakhel

Department of Physics, College of Science, University of Bahrain, P.O. Box 32038, Sakhir, Kingdom of Bahrain

adakhil@uob.edu.bh

ORCID: 0000-0001-7251-6055

Abstract

In the present work, pristine and Ni^{2+}/Al^{3+}- codoped anatase (TiO_2) nanocomposite powders were synthesized by the thermal co-precipitation method. The samples were characterized by several techniques. The X-Ray diffraction (XRD) was used for structural characterization and the optical absorption spectroscopy was used for the optical characterization. The structural/optical studies proved the formation of a substitutional solid solution (SSS). The magnetization measurements were performed to investigate the magnetic properties of the synthesized samples. In the present work, nickel (Ni^{2+}) dopant ions were used to introduce stable ferromagnetic (FM) properties into the synthesized anatase, while Al^{3+} dopant ions were utilized to supply itinerant electrons necessary to support and boost the created FM properties. The roadmap of the present work was to establish the hydrogenation conditions necessary to create ferromagnetic (FM) properties in the host codoped samples and study the effect of hydrogenation temperature on the parameters of the created FM properties, especially the magnetic energy (U_{mag}) and saturation magnetization (M_{sat}). It was found that the created FM properties in Ni/Al-doped TiO_2 nanocomposite powder by using the hydrogenation effect could be enhanced and controlled *via* the temperature of the hydrogenation (T_H). The experimental results revealed that U_{mag} of TiO_2:Ni:Al system increased by ~241% and the saturation magnetization by ~140% with increasing of T_H by 100 ºC (from 400 ºC to 500ºC). The obtained saturation magnetization (M_{sat}) of 1.09 emu/g and magnetic energy (U_{mag}) of 42.6 erg/g were higher than the previously obtained values for created Ni-doped TiO_2 by ~50 times. Such great novel results were obtained due to dealing with two factors; the Al^{3+} ions as co-dopant, which can supply an excess of itinerant electrons that boost the ***S.S*** Heisenberg interactions in addition to choosing a suitable temperature of hydrogenation.

Keywords: Ni-Al codoped TiO_2; Creation of ferromagnetism; hydrogenation; TCO-DMS materials.

1. Introduction

Titanium dioxide belongs to the transparent conducting oxide (TCO) family. It has received great consideration as a multifunctional material widely used for various devices, such as optoelectronics, solar cells, transparent electrodes, gas sensors, and photocatalysis, because of its excellent electro-optical properties [1-6]. Moreover, the developments in the properties of TiO_2-based materials are the subject of nowadays.

Pristine Ti dioxide is a wide-band semiconductor with an indirect bandgap of ~ 3 -3.2 eV [7,8]. It crystallizes in three possible crystalline structures: anatase [A], rutile [R], and brookite [B] depending on the preparation conditions and temperature [9,10]. The photocatalytic, electrical, optical, and other properties of Ti oxide can be controlled through doping with different ions [11-14]. Besides, the properties of Ti oxide can be managed by organizing its natural point defects, like oxygen (O) vacancies and Ti interstitials. Moreover, it was found that doping could create exotic properties. For example, doping with transition metal (TM) or rare-earth (RE) ions could create ferromagnetic (FM) properties converting the host TiO_2 material into diluted magnetic semiconductors (DMS), which widen its applications.

It is noteworthy that, weak FM behaviour could be easily created in synthesized TCO samples even without doping, which symbolized as a d^0FM phenomenon [15, 16]. The d^0FM phenomenon is attributed to the presence of structural point defects like O-vacancies in the nanocrystallites. The O-vacancies can capture itinerant electrons, creating local moments, which lead to some kind of weak magnetic spin-spin ($S.S$) Heisenberg responses [17-21]. The d^0FM phenomenon was proved to be unstable and could be removed thermally [22].

In the present work, anatase TiO_2 nanopowder samples codoped with Ni^{2+} and Al^{3+} ions were synthesized to construct DMS. Nickel dopant ions are used to introduce stable ferromagnetic (FM) properties into the anatase powder sample, while Aluminum dopant ions are used to supply itinerant electrons necessary to support and boost the created FM properties. According to the 6-coordination ionic radii table [23], the radii difference between Ni^{2+}(0.069 nm) and Ti^{4+}(0.06 nm) ions is ~13% and between Al^{3+}(0.054 nm) and Ti^{4+} is ~10%. Thus, the possible ionic substitutions Ni_{Ti} and Al_{Ti} cannot cause a significant geometrical distortion in the TiO_2 host lattice, according to the Hume-Rothery (H-R) rules. Therefore, ions Ni^{2+} and Al^{3+} can easily be doped in the TiO_2 crystal forming a substitutional solid solution (SSS). Moreover, it is also possible to believe that some amount of Ni and Al dopant ions might occupy interstitial positions and reside in crystallite boundaries.

The strength of the spin-spin ($S.S$) interaction between Ni^{2+} dopant ions that could create the FM properties significantly depends on the effective interionic separation (R) as well as the local permittivity of the host TiO_2 crystalline medium (ECM) necessary to switch on the $S.S$ Heisenberg interaction. Therefore, it is possible to control the created magnetic properties of the DMSs through

the dopant kind and concentration and by catalyzing the **ECM** to permit/boost the **S.S** interaction. In the present work, the action used to catalyze the **S.S** interaction is the hydrogenation process. The H_2 molecules should be dissociated into H-species under the impact of Ni^{2+} dopant ions [24]. The H-species can create O-vacancies, which stimulate the **ECM** to permit the **S.S** interaction. The Al ions dopant can supply the itinerant electrons that support and boost the **S.S** interaction. The effect of hydrogenation temperature on the created FM parameters especially the magnetic energy (U_{mag}) and saturation magnetization (M_{sat}) is the purpose to measure in the present study.

2. Experimental details

The road map of the present investigation began with the synthesis of pristine and Ni/Al-codoped TiO_2 (TiO_2:Ni:Ga) nano-powders by thermal co-precipitation method. The starting analar materials for the synthesize were titanium tetrachloride ($TiCl_4$) liquid, nickel (II) chloride ($NiCl_2.6H_2O$), and aluminum nitride ($Al(NO_3)_3$) (from Sigma-Aldrich Chemical Company). The molar ratios of Ni/Ti and Al/Ti were ~ 4.8 %. The procedure of synthesis was discussed elsewhere. In brief, the precursor was prepared from a mixture solution of 3 ml $TiCl_3$, ~ 30 ml ethanol, ~ 120 ml bi-distilled deionized water, with the appropriate amounts of $NiCl_2.6H_2O$, and $Al(NO_3)_3$ in a glass beaker. The solution was kept under magnetic stirring for ~2-3h at room temperature, and then the temperature was slowly increased to ~ 60-80 ^oC with continuous stirring until a precipitate powder was obtained. Finally, the powder was flash sintering in a closed oven at 500 ^oC for 1 hr, followed by a slow cool to the room temperature. The present syntheses lead to the formation of a single phase of the TiO_2 structure. Finally, the powder was palletized under ~8 tons for characterization. The reference un-doped TiO_2 powder was also synthesized by a similar procedure. Amounts from each synthesized fine powder were annealed in the H_2-gas atmosphere at the 400 ^oC and 500 ^oC for 20 min. It is noteworthy that such hydrogenation at high-temperature 500^oC could not reduce TiO_2 to Ti since TiO_2 is very stable oxide and it is difficult to reduce it. The prepared samples were referred to as; TiO_2-H, TiO_2:Ni:Al-H (for 400^oC), and TiO_2:Ni:Al-HH (for 500^oC), respectively.

The crystalline structures were investigated by the X-ray diffraction (XRD) method that carried out with a Rigaku Ultima-VI X-ray diffractometer (Cu K_α). The obtained XRD results were analyzed by the Rietveld profile refinements (RPR) method through a built-in PDXL2 (ver.2.0.3.0) program. The spectral optical properties of the powder samples were measured by Shimadzu UV-3600 double beams spectrophotometer that equipped with an integrating sphere for diffuse reflectance spectroscopy (DRS) measurements in the range of 200 nm - 830 nm. The magnetic properties of the synthesized samples were measured at room temperature by a vibrating sample magnetometer type VSM-PMC Micro-Mag 3900.

3. Structural analysis

The crystal structure of the synthesized samples (TiO$_2$, TiO$_2$:Ni:Al, TiO$_2$-H, TiO$_2$-Ni-Al-H, and TiO$_2$-Ni-Al-HH) were investigated by the X-ray diffraction (XRD) method and the results are shown in Fig.1a. The built-in "Rietveld refinements fitting -PDXL2" program was used to analyze the obtained XRD patterns. The starting models for the structural analysis were anatase [A], rutile [R], and brookite [B]. However, the main crystal structure of the pristine and codoped Ti oxide, shown in Fig.2, was found to be anatase [A] with traces from [R] and [B] phases. The extracted lattice parameters given in table:1 are close to the known parameters of the tetragonal [A] phase of space group (SG) I4$_1$/amd of parameters a=b=3.784 Å, c=9.515Å [25] or with the JCPDS 21-1272 angles 2θ =25.3^o, 37.7^o, 47.8^o, 54°, 62.7^o. [26]. However, one weak hump was observed at 2θ ~ 31.07^o with FWHM ~ 0.99^o and identified to be (211) reflection of a tiny amount of nano brookite [B] phase (Orthorhombic: Pbca, a=9.184 Å, b=5.557 Å, c=5.154 Å [25]) of crystallite size ~ 8.7 nm. In addition, weak humps from a tiny amount of rutile [R] phase (tetragonal: P4$_2$/mnm, a=b=4.5936 Å, c=2.9587 Å [25]) was also observed in Fig.1a. In general, the anatase phase [A] continued to be almost the unique phase even with co-doping and hydrogenation.

The graphical representation by the Rietveld refinements program for TiO$_2$:Ni:Al sample is demonstrated in Fig.1b, where; the red solid line (up) is the experimental data, the solid blue line (up) is the calculated pattern and the solid pink line (down) is the intensity difference between the experimental and calculated patterns. The Rietveld fitting parameters [R_{wp} (%)−weighted profile and S(%)−goodness-of-fit] indicated very well fittings; since S ~ 1 [27]. Fig.1b shows the Rietveld refinements fitting for the TiO$_2$:Ni:Al sample of [A] phase, as an example of an excellent phase fitting (S=1.16). The structural analyses, including the average crystallite size (*CS*) and the microstrain (ε), were calculated through the built-in software according to Halder-Wagner (H.W) method[28]:- $(\beta_{hkl} / \tan\theta_{hkl})^2 = (k\lambda / D)(\beta_{hkl} / \tan\theta_{hkl} \sin\theta_{hkl}) + 16\varepsilon^2$,where θ$_{hkl}$ is the Bragg's angle of (hkl) reflection, λ is the Cu K$_\alpha$ wavelength, kλ=2.05Å, D is the CS, ε is the lattice microstrain, and β$_{hkl}$(rad) is the peak half-width. Thus, the average CS and ε could be determined from the straight-line plot of $Y = (\beta_{hkl} / \tan\theta_{hkl})^2$ vs. $X = (\beta_{hkl} / \tan\theta_{hkl} \sin\theta_{hkl})$, as shown in Fig.1c for TiO$_2$:Ni:Al sample. The calculated values of CS and ε for all studied samples are presented in Table:1. The first observation is that the calculated CS reveals that the synthesized samples consist of nanometric crystallite size in the range of 5 - 7 nm.

The absence of any XR-reflection related to the pure or compound of Ni and Al dopant ions confirms that the dopant ions dissolved in TiO$_2$ lattice and did not aggregate or reacted with the sample's mother ions. Thus, the dopant Ni and Al ions formed SSS within TiO$_2$, which confirms the prediction mentioned in the "introduction" that based on the geometrical H-R rule.

The XRD patterns of the hydrogenated samples were demonstrated in Fig.1a. It is clear that the hydrogenations (H and HH) did not change the main phase structure [A] of any sample. However, a slight boosting of the [R]-phase content at the expense of the [A] phase was detected to be happening due to the hydrogenation, especially for the HH sample. The relative ratio of the strongest intensities of [R]:(110) to [A]:(101), (I_R/I_A) was ~ 11% and 14% for TiO2:Ni:Al-H and TiO2:Ni:Al-HH, respectively. This result might attribute to the increase in the formed O-vacancies by the increasing of the hydrogenation temperature (T_H).

Data analysis revealed that the present codoping caused a decrease in the unit-cell volume since both incorporated Ni^{2+} and Al^{3+} dopant ions are smaller than Ti^{3+} ion. Moreover, the difference in sizes of solute (Ni and Al) ions and solvent (Ti) ions cause increase in microstrain (ε) from 0.03 to 0.7, as given in table:1. These variations confirmed the formation of SSS. Another observation is that the hydrogenation slightly increased the unit-cell volume by the formation of O-vacancies.

4. Optical analysis

The spectral optical properties of the synthesized powders were studied through the measurements of the diffuse reflectance $R(\lambda)$ spectroscopy (DRS) in the range of 250 – 800 nm by utilizing the standard spectral reflectance from BaSO4 powder (supplied by Shimadzu company). The spectral Kubelka-Munk (K-M) absorption function $F(\lambda)$ was calculated by $F(\lambda) = \left(1 - R(\lambda)\right)^2 / 2R(\lambda)$ [29], as shown in the inset of Fig.2. The main absorption region ~ 400-500 nm was focused to estimate the threshold absorption edge (E_{th}), which is almost equivalent to the band gap (E_g) and is given in table:1. The absorption edge of the un-doped TiO2 was found ~3.1 eV, which is consent with the known range of bandgaps: 3-3.2 eV [8, 30]. The band gap of host TiO2 suffered narrowing (BGN) due to the codoping by Ni^{2+}/Al^{3+} ions, which generated structural point defects including O-vacancies for local charge neutrality. The energy levels of the generated defects lay in the bandgap, close to and merged with the bottom of the host TiO2 conduction band causing a decrease in band gap - Urbach effect [31].

The spectral absorption function $F(\lambda)$ of the hydrogenated samples (TiO2-H, TiO2:Ni:Al-H, and TiO2:Ni:Al-HH) are shown in Fig.2. It is clear that the hydrogenation introduced hefty changes inside the bandgap of codoped TiO2. Fig.2 reveals that the bandgap of the hydrogenated codoped TiO2 is substantially filled with energy levels of the created defects. Moreover, the hydrogenation enhanced the absorption $F(\lambda)$ in the high-wavelength (NIR) part of the absorption spectrum of the doped samples, so that $F(\lambda)$ is directly proportional to λ according to the relation, $F(\lambda) \sim \lambda^p$ (where $p >$ 0), as shown in fig.3 " * ". Such behaviour is usually attributed to the absorption of free-carriers (itinerant electrons) and attributed by the highly generated O-vacancies that noticeably increased the free-carrier concentration [32 - 36].

The hydrogenation creates dense O-vacancies and itinerant electrons in doped TiO$_2$, which causes an increase in the optical absorption A(λ) in the NIR spectral region (fig.3). Data on table:1 shows that the hydrogenation of un-doped and the co-doped TiO$_2$ samples shifted their threshold edges (E_{th}) to higher energies of different magnitudes. For the un-doped TiO$_2$-H sample, the blue shift in E_{th} is attributed to the reduction in the density of structural defects: imperfection, dislocation, dangling bonds, etc., causing cutback in the Urbach tail that increased in E_{th}. However, for co-doped TiO$_2$ sample, the blue shift in the measured optical bandgap is attributed mostly to the increase in carrier concentration following the Moss-Burstein (B-M) mechanism [37]. During the hydrogenation process of the host TiO$_2$ under the impact of dopant Ni^{2+} ions, some H$_2$ molecules should be dissociated into H-species (atoms/ions) [24], which, in turns removed some structural oxygen creating/densifying O-vacancies with itinerant electrons. Dopant ions play the role of the internal catalyst in the dissociation of H$_2$ molecules.

It is worth noting that such an increase in free (itinerant) electrons concentration should support the *ECM* to switch on the *S.S* interaction and, hence create/enhance the FM properties.

5.

5.1- Investigation of the as-prepared samples:

The pristine anatase TiO$_2$ was known to have diamagnetic (DM) properties [38, 39]. However, the synthesized un-doped TiO$_2$ of the present work has PM behaviour of small susceptibility (~10^{-7}cgs/g), as presented in Table:2. Similar behaviour was also observed earlier [38,39]. The PM properties were attributed to the created structural point defects, including O-vacancies. In general, the point defects can generate PM or weak FM properties [20] depending on their concentration, distribution, and separations.

The PM behaviour of TiO$_2$ nano-powder in the present work maintained even with codoping. However, the incorporation of Ni/Al ions in the host TiO$_2$ caused a remarkable increase in the **susceptibility by ~ 10 times**. The PM susceptibility of TiO$_2$:Ni:Al sample can be used to estimate the average effective para-magnetic moment per dopant Ni ion interacted paramagnetically with the applied field by using Curie law for mass susceptibility (per g): $\chi(per\ g) = N_{Ni}\ \mu_{Ni}^2 / 3\rho k_B T$, where, μ_{Ni}

is the para-magnetic moment per dopant Ni ion, k_B is the Boltzmann constant, ρ is the density of host TiO$_2$, and T is the working temperature. Thus, μ_{Ni} is equal to 3.38μ_B for TiO$_2$:Ni:Al, where μ_B is the Bohr magneton. However, the known experimental paramagnetic moment of Ni(II) ion in some octahedral complexes was 2.9-3.3μ_B [40]. Therefore, almost all the incorporated Ni^{2+} dopant ions participated in the observed PM interaction. To attain the spin-spin *S.S* Heisenberg exchange interaction between dopant Ni^{2+} ions, the average interionic separation (R) between them should be less than (1.5×a), where (a) is the TiO$_2$ lattice parameter [41,42] in addition to the proper local

permittivity of the host TiO$_2$ crystalline medium (ECM), which intermediate the **S.S** interaction. For uniform distribution of Ni^{2+} dopant ions throughout the host TiO$_2$ lattice, the average interionic separation (R) can be estimated by; $N_{ion}V=1$, where N_{ion} is the Ni^{2+} concentration (1.37×10^{21} cm^{-3}) and V= (4/3)πR^3, thus R ~ 0.56 nm, which almost equal to 1.5×a. Moreover, the concentration of Ni^{2+} ions is much less than that of anatase unit cells, C$_{cell}$= V_{cell}^{-1} = 7.40x10^{21} cm^{-3}. Therefore, due to the distance separation between dopant Ni^{2+} ion, the **S.S** interaction between neighbouring Ni^{2+}-Ni^{2+} dopant ions could not be switched-on confirming the observed results unless stimulate the anatase ECM for the super-exchange interaction between the Ni^{2+}-Ni^{2+} dopant ions. Such stimulation was successfully achieved in the present work by the hydrogenation process.

5.2- Investigation of hydrogenated samples

The magnetic study of the hydrogenated synthesized un-doped TiO$_2$-H sample at room temperature (RT) revealed the creation of weak FM properties superimposed on the major DM behavior. The FM component of TiO$_2$-H behavior is shown in Fig.3. Such a weak d^{0}FM phenomenon (explained in the introduction) could be generated by the internal structural point defects, like O-vacancies, which mainly created by hydrogenation [20].

The FM parameters (H$_c$: coercive force, M$_r$: remanence, and M$_{sat}$: saturation magnetization) extracted from hysteresis loops are given in table:2. Moreover, the magnetic energy (U$_{mag}$) was calculated to compare the quality of the FM hysteresis behaviours for one magnetic system and considered as a figure-of-merit, FOM=U$_{mag}$=H$_c$M$_r$ (erg/g) [43]. The magnetic energy U$_{mag}$ of un-doped TiO$_2$ was weak (0.12 erg/g) and it is unstable and could be thermally removed.

It is clear that the hydrogenation has an amazing effect on the magnetic properties of SSS-TiO$_2$:Ni:Al, which under the impact of Ni dopant could create RT-FM through controlling over the *ECM*. The created FM parameters are presented in table:2. The M$_{sat}$ values can be used to estimate the effective ferro-magnetic moment of dopant Ni^{2+} ions participated in the FM properties through the following equation: $\mu_{Ni^{2+}}^{eff} = M_{sat}(emu/g) \times D/N_{Ni^{2+}}(cm^{-3})$, where D is the density of host TiO$_2$ (4.23 g.cm^{-3}) and $\mu_{Ni^{2+}}^{eff}$ is the effective FM moment of *Ni^{2+}* ions. Thus, $\mu_{Ni^{2+}}^{eff} = 0.37\mu_B$, which is less than the known value 0.60μ_B for the FM moment extracted from the saturation measurements of the pure Ni metal at RT. Thus, only ~ 62% of the dopant Ni^{2+} ions could participate in the creation of FM behaviour. Such participation fraction is attributed to the nature of the synthesized nano-crystallites powder samples; some doped Ni ions were not Ferro-magnetically interacted with each other and might accumulate on the crystallite boundaries (CBs) in the form of ions with different oxidation numbers. In general, the present experiments prove that such creation of FM is directly related to the created structural point defects like O-vacancies and thus depends on the hydrogenation parameters.

Under the impact of Ni^{2+} dopant ions, the H_2 molecules, during the hydrogenation process, could be dissociated into hydrogen H-species [24]. The hydrogen acts as a reducing agent because it donates its electrons to the crystal creating structural O-vacancies, which assist the mediation of the super-exchange $S.S$ interaction necessary for the realization of FM behavior. Thus, the hydrogenation that densifies the O-vacancies and the itinerant electrons in *ECM*, is a necessary and sufficient condition to create FM properties at RT. Therefore, the strength of the created FM should be dependent on the hydrogenation conditions [the duration, Δt, and temperature, T_H]. Consequently, the effect of the hydrogenation temperature T_H on the strength of the created FM properties was studied in the present work by using two temperatures $T_H = 400^oC$ (for H sample) and $T_H = 500\ ^oC$ (for HH sample) and the obtained corresponding hysteresis loops are shown in fig.3.

Data of table:2 demonstrates that when the temperature T_H increased by 100 ^oC (from 400^oC to 500 ^oC) then the U_{mag} of TiO$_2$:Ni:Al system increased by 3.4 times and the M_{sat} increased by 1.4 times. So, the increase of T_H causes an increase in the density of O-vacancies, which, in turn, increases the "**bridges of overlapping**" between the spins ($S.S$) of the Ni^{2+} dopant ions. Therefore, the host *ECM* plays a significant role in controlling the energy of the $S.S$ interaction.

Due to the procedure of the present work, especially the impact of Al co-dopant and apply suitable conditions of hydrogenation, the results of the created FM properties are very improved comparing to the results obtained by previous works. The saturation magnetization M_{sat} for Ni-doped TiO$_2$ was 0.044 memu/g [44], 0.020 emu/g [45], 0.021emu/g [46], and for (Ni+Fe)-codoped TiO$_2$ sample the result was 0.160 emu/g [47].

6. Conclusions

Pristine and Ni/Al-codoped TiO$_2$ nanocomposites were successfully synthesized by the thermal co-precipitation method to fabricate DMS solid solution (SSS) material. The structural and optical properties of the samples were systematically investigated to confirm the formation of SSS. Nickel dopant ions are used to introduce stable ferromagnetic (FM) properties for the synthesized anatase nano-powder sample, while the aluminum dopant ions are utilized to supply itinerant electrons necessary to support and boost the created FM properties. The samples were hydrogenized at two temperatures (400 ^oC and 500 ^oC). Thus, the studied nanocomposite samples were: TiO$_2$, TiO$_2$:Ni:Al, TiO$_2$-H, TiO$_2$:Ni:Al-H, and TiO$_2$:Ni:Al-HH. The effect of hydrogenation temperature on the created FM parameters especially the magnetic energy (U_{mag}) and saturation magnetization (M_{sat}) was the purpose of the present study. Novel results about the boosting of the created FM were obtained by using a suitable hydrogenation temperature (T_H). The values of 1.09 emu/g for M_{sat} and 42.6 erg/g for magnetic energy (U_{mag}) were achieved when $T_H = 500\ ^oC$. These values are higher by ~50 times than those obtained for previous investigations on Ni-doped TiO$_2$. The experimental Data revealed that

U_{mag} of the hydrogenated TiO_2:Ni:Al system increased by 241% and the magnetization increased by 140% with increasing of T_H by 100 ºC (400 ºC – to -500ºC).

Such great novel results obtained due to two factors: using Al^{3+} ions co-doping as a supplier of itinerant electrons that boost the ***S.S*** Heisenberg interactions and choosing the appropriate temperature of hydrogenation.

No conflict of interest exists:

I wish to confirm that there are no conflicts of interest associated with this publication and there has been no significant financial support for this work that could have influenced its outcome.

Caption of tables

Table:1 lattice microstrain (ε), Crystallite size (CS), Lattice parameters (a=b and c), unit-cell volume (V_{cell}), Rietveld refinement parameters, RP (R_{wp} and S), and threshold optical absorption (E_{th}) of the synthesized nanocomposite powders.

Table:2 Magnetic parameters of the synthesized nanocomposite powders; PM susceptibility (χ) and FM parameters (H_c: coercive force, M_r: remanence, M_s: saturation magnetisation, and magnetic energy, U_{mag}.)

Caption of figures

Fig.1a: XRD patterns of the synthesized nanopowders; TiO2, TiO2:Ni:Al, TiO2-H, TiO2:Ni:Al-H, and TiO2:Ni:Al-HH. Anatase is the major phase crystallised.

Fig.1b: Graphical representation of the Rietveld refinements for TiO2:Ni:Al sample, where; the red solid line (up) is the experimental data, the blue solid line (up) is the calculated pattern, and the solid pink line (down) is the intensity difference between the calculated and registered.

Fig.1c: H-W plot for TiO2:Ni:Al sample

Fig.2: Spectral K-M absorption function; $F(\lambda)$ of the hydrogenated samples. The thresholds of absorption are shown. The inset shows is the function absorption function $F(\lambda)$ of the synthesized samples (TiO2 and TiO2:Ni:Al)

Fig.3: M(H) relationship for the hydrogenated samples.

Table 1:

| Sample | ε (%) | CS (nm) | a, b, c (Å) | V_{cell} (Å^3) | R.P | | E_{th} (eV) |
					R_{wp}(%)	S	
TiO$_2$	0.03	5.8	a=b=3.7732, c=9.484	135.02	27.7	1.30	3.10
TiO$_2$:Ni:Al	0.7	6.8	a=b= 3.774, ,c=9.460	134.7	29.76	1.16	2.70 (vis)
Hydrogenated samples							
TiO$_2$-H	~ 0	4.8	a=b=3.779, c = 9.499	135.7	25.39	1.45	3.17
TiO$_2$:Ni:Al-H	0.7	6.9	a=b= 3.780, c=9.460	135.1	25.21	1.22	3.28
TiO$_2$:Ni:Al-HH	~0.0	5.8	a=b=3.784 , c=9.482	135.7	26.35	1.28	3.28

Table:2

Sample	Behaviour	H_c (Oe)	M_r (memu/g)	M_{sat} (memu/g)	U_{mag}(erg/g)
TiO$_2$-H	DM+ Weak FM	185.7	0.5	2.2	0.09
TiO$_2$:Ni:Al-H	FM	54.6	228.6	781.5	12.48
TiO$_2$:Ni:Al-HH	FM	107.3	397.2	1092.1	42.60
		χ (cgs/g)			
TiO$_2$	Weak PM	3.4×10^{-7}			
TiO$_2$:Ni:Al	PM	2.62×10^{-6}			

References

[1] N. Rahimi, R. A.Pax, E. Mac. A.Gray, Review of functional titanium oxides. I: TiO_2 and its modifications, Progress in solid state chemistry 44(3)(2016) 86-105., https://doi.org/10.1016/j.progsolidstchem.2016.07.002

[2] D. Reyes-Coronado, G. Rodrıguez-Gattorno, M. E. Espinosa-Pesqueira, C. Cab, R. de Coss and G. Oskam, Phase-pure TiO2 nanoparticles: anatase, brookite and rutile, Nanotechnology 19 (2008) 145605 (10pp)

[3] A. Balhamri, A. Deraoui, Y. Bahou, M. Rattal, Az. Mouhsen, M. Harmouchi, A. Tabyaoui and E. M. Oualim, Surface and optical properties of zinc oxide doped with fluor synthesized by magnetron sputtering: applications in transparent conductive oxides (TCO), Int. J. Thin. Fil. Sci. Tec. 4(3)(2015) 205-210,   http://dx.doi.org/10.12785/ijtfst/040308

[4] J. Dong, J. Han,Y. Liu, A. Nakajima, S. Matsushita, S. Wei, W. Gao, Defective black TiO_2 synthesized via anodization for visible-light photocatalysis. Appl. Mater. Inter. 6 (2018)1385-1388.

[5] D. V. Bavykin,V. N. Parmon, A. A. Lapkin, F. C. Walsh, The effect of hydrothermal conditions on the mesoporous structure of TiO_2 nanotubes. J. Mater. Chem. 14 (2004) 3370-3377.

[6] H. -F. Zhuang, C. -J. Lin, Y. -K. Lai, L. Sun, J. Li, Some Critical Structure Factors of Titanium Oxide Nanotube Array in Its Photocatalytic Activity, Environ. Sci. Technol. 41 (2007) 4735- 4740.

[7] Xuefeng Lu, Tingting Zhao, Xu Gao, Junqiang Ren, Xiaobin Yan, and Peiqing La, Investigation of Mo-, Pt-, and Rh-doped rutile TiO_2 based on first-principles calculations, AIP Advances 8 (2018) 075014; https://doi.org/10.1063/1.5038776

[8] Y. Ma, X. Wang, Y. Jia, X. Chen, H. Han, C. Li, Titanium dioxide-based nanomaterials for photocatalytic fuel generations,Chem. Rev. 114 (2014) 9987-10043.

[9] J. Tian, H. Gao, H. Deng, L. Sun, H. Kong, P. Yang, J. Chu, Structural, magnetic and optical properties of Ni-doped TiO_2 thin films deposited on silicon(1 0 0) substrates by sol–gel process , J. Alloys Compd. 581 (2013) 318–323.

[10] M. Manzoor, A. Rafiq, M. Ikram, M. Nafees, S. Ali, Structural, optical, and magnetic study of Ni‑doped TiO_2 nanoparticles synthesized by sol–gel method, Int. Nano Letters 8 (2018)1–8.

[11] X. Chen, S. S. Mao, Titanium dioxide nanomaterials: synthesis, properties, modifications, and applications. Chem. Rev. 107 (2007) 2891–2959

[12] U. Diebold, The surface science of titanium dioxide. Surf. Sci. Rep. 48(2003) 53–229.

[13] A. C. M. Padilha, H. Raebiger, A. R. Rocha and G. M. Dalpian, Charge storage in

oxygen deficient phases of TiO2: defect Physics without defects,
Sci. Rep. 6 - 28871(2016)1-6.

[14] Y. Xu, C. Zhang, L. Zhang, X. Zhang, H. Yao, J. Shi, Pd-catalyzed instant
hydrogenation of TiO2 with enhanced photocatalytic performance Energy,
Environ. Sci. Technol. 9 (2016) 2410-2417

[15] Mohamed Bououdina, Aqeel Aziz Dakhel, Mohammad El-Hilo, Dalaver H. Anjum,   Mohammed
Benali Kanoun,   and Souraya Goumri-Said, Revealing a room temperature ferromagnetism in
cadmium oxide nanoparticles: an experimental and first-principles study,
RSC Adv. 5 (2015) 33233–33238.

[16] B. Qi, S. Olafsson and H. P. Gislason, Vacancy defect-induced d0 ferromagnetism in
undoped ZnO nanostructures: Controversial origin and challenges,
Prog. Mater. Sci. 90 (2017) 45-74.

[17] G. Feng, W. Shufen, C. Hongming, L. Chunzhang, Synthesis and optical properties of SnO2
nanorods, Nanotechnology 19 (2008) 095708.

[18] S. Kumar, Y. J. Kim, B. H. Koo, S. Gautam, K. H. Chae, R. Kumar, C. G. Lee, Room
temperature ferromagnetism in chemically synthesized ZnO rods,Mater. Lett. 63 (2009) 194-196.

[19] I. S. Elfimov, S. Yunoki, G. A. Sawatzky, Possible Path to a New Class of Ferromagnetic and
Half-Metallic Ferromagnetic Materials, Phys. Rev. Lett. 89 (2002) 216403.

[20] S. Zhou, E. Cizmar, K. Potzger, M. Krause, G. Talut,M. Helm, J. Fassbender, S. A. Zvyagni,
J. Wasnitza, H. Schmidt, Origin of magnetic moments in defective TiO2 single crystals,
Phys. Rev. B 79 (2009) 113201.

[21] A. A. Dakhel, M. Bououdina, Structural, optical, and magnetic properties of Cu- and
Ni-codoped CdO dilute magnetic nanocrystalline semiconductor: effect of hydrogen
post- treatment, Appl. Phys. A 119 (2015)1053–1060.

[22] A. A. Dakhel, Critical role of hydrogenation for creation of magnetic Cd–Cu co‑incorporated
TiO2 nanocrystallites, Applied Physics A 126 (2020) 41 (8 pages).

[23] R. D. Shannon, Revised effective ionic radii and systematic studies of interatomic distances in
halides and chalcogenides, Acta Crystallogr. A 32 (1976) 751-767.

[24] M. Pozzo, D. Alfe, Hydrogen dissociation and diffusion on transition metal (=Ti, Zr,
V, Fe, Ru, Co, Rh, Ni, Pd, Cu, Ag)-doped Mg (0001) surface,
Int. J. Hydrogen Energy 34 (2009) 1922 - 1930.

 [25] S. M. Gupta, M. Tripathi, A review of TiO2 nanoparticles, Chinese Sci. Bulletin 56 (2011)
1639-1657. DOI: 10.1007/s11434-011-4476-1

[26] P. W. Atkins, T. L. Overton, J. P. Rourke, M. T. Waller, F. A. Armstrong, Inorganic
Chemistry, 5th ed., University press-Oxford, OX2 6DP, UK, 2010,

Web: Inorganic Chemistry - Mark Weller, Tina Overton, Jonathan Rourke, Fraser
Armstrong - Google Books.mht

[27] L. B. McCusker, R. B. Von Dreele, D. E. Cox, D. Louer, P. Scardi, Rietveld refinement
guidelines, J. Appl. Cryst. 32 (1999) 36.

[28] A. Khorsand Zak, W. H. Abd Majid, M. E. Abrishami, R. Yousefi, X-ray analysis of
ZnO nanoparticles by Williamson–Hall and size–strain plot methods,
Solid State Sci. 13 (2011) 251–256.

[29] A. E. Morales, E. S. Mora, and U. Pal, Use of diffuse reflectance spectroscopy for optical
characterization of un-supported nanostructures, Revista Mexicana de Fisica S53 (2007) 18-22.

[30] Daniela Sojic, Vesna Despotovic, Biljana Abramovic, Nadia Todorova, Tatiana Giannakopoulou,
and Christos Trapalis, Photocatalytic degradation of mecoprop and clopyralid in aqueous
suspensions of nanostructured N-doped TiO$_2$,   Molecules 15 (2010) 2994-3009;
doi:10.3390/molecules15052994.

[31] F. N. C. Anyaegbunam, C. Augustine, A study of optical gap associated Urbach energy tail
of chemically deposited metal oxides binary films, Dig. J. Nanomater. Bios.13 (2018) 847-856.

[32] S. C. Baker-Finch, K. R. McIntosh, Di Yan, K. C. Fong, Near-infrared free carrier
absorption in heavily doped silicon, J. Appl. Phys. 116 (2014) 063106 (12 pages).

[33] A. A. Dakhel, A. Y. Ali-Mohamed, Optical and transport phenomena in CdO: La films prepared
by sol-gel method, J. Sol-Gel Sci. Technol. 44 (2007) 241–247

[34] H. L. Hartnagel, A. L. Dawar, A. K. Jain, G. Jagadish, Semiconducting Transparent Thin Films,
IOP, Bristol, 1995.p. 226.

[35] Z. Qiao, C. Agashe, D. Mergel, Dielectric modeling of transmittance spectra of thin ZnO:Al
Films, Thin Solid Films **496**, 520 (2006).

[36] Le Yuan, Xiaolong Weng, Ming Zhou, Qingyong Zhang, and Longjiang Deng, Structural and
Visible-Near Infrared Optical Properties of Cr-Doped TiO$_2$ for Colored Cool Pigments,
Nanoscale Res Lett. **12**, 597 (2017). doi: 10.1186/s11671-017-2365-5

[37] S. C. Baker-Finch, K. R. McIntosh, Di Yan, K. C. Fong, Near-infrared free carrier
absorption in heavily doped silicon, J. Appl. Phys. 116 (2014) 063106 (12 pages).

[38] H. Wang, J. Wei, R. Xiong, J. Shi, Enhanced ferromagnetic properties of Fe+N codoped TiO2
anatase, J. Magn. Magn. Mater 324 (2012) 2057-2061.

[39] Anand Kumar , Manish K. Kashyap , Namita Sabharwal, Sarvesh Kumar , Ashok Kumar,
Parmod Kumar, K. Asokan, Structural, optical and weak magnetic properties of Co and Mn
codoped   TiO2 nanoparticles, Solid State Sciences 73 (2017) 19-26.

[40] The web page of the University of the West Indies at Mona, Jamaica, The Dept. of
Chemistry, http://wwwchem.uwimona.edu.jm/spectra/MagMom.html. accessed May. 2020.

[41] L. Bergqvist, O. Eriksson, J. Kudrnovsky, V. Drchal, P. Korzhavyi, L. Turek, Magnetic Percolation in Diluted Magnetic Semiconductors, Phys. Rev. Lett. 93(2004) 137202.

[42] S. -Y. Seo, C. -H. Kwak, S. -H. Kim, S. -H. Park, I. -J. Lee, S .-W. Han, Synthesis and characterization of ferromagnetic Zn1-xCoxO films, J. Cryst. Growth 346 (2012) 56.

[43] V. Raghavan, Materials Science and Engineering: A first course, 5th ed., 2004, Prentic-Hall of India private limited, New Delhi, P.406.

[44] Sandeep Kumar Singh Patel, Paramananda Jena, N.S. Gajbhiye, Structural and room-temperature ferromagnetic properties of pure and Ni-doped TiO_2 nanotubes, Materials Today: Proceedings 15 (2019) 388–393

[45] Qing Wang, Xiaoming Liu, Xuegang Wei, Jianfeng Dai, and Weixue Li, Ferromagnetic Property of Co and Ni Doped TiO_2 Nanoparticles, J. Nanomater. , Volume 2015, Article ID 371582, 5 pages, http://dx.doi.org/10.1155/2015/371582

[46] M. Manzoor, A. Rafiq, M. Ikram, M. Nafees, S. Ali, Structural, optical, and magnetic study of Ni‑doped TiO2 nanoparticles synthesized by sol–gel method, Int. Nano Lett. 8 (2018)1–8.

[47] Salma Waseem, Safia Anjum, Lubna Mustafa, Tallat Zeeshan, Zohra Nazir Kayani, Khalid Javed, Structural, magnetic and optical investigations of Fe and Ni co-doped TiO_2 dilute magnetic semiconductors, Cer. Int. 44 (2018) 17767–17774
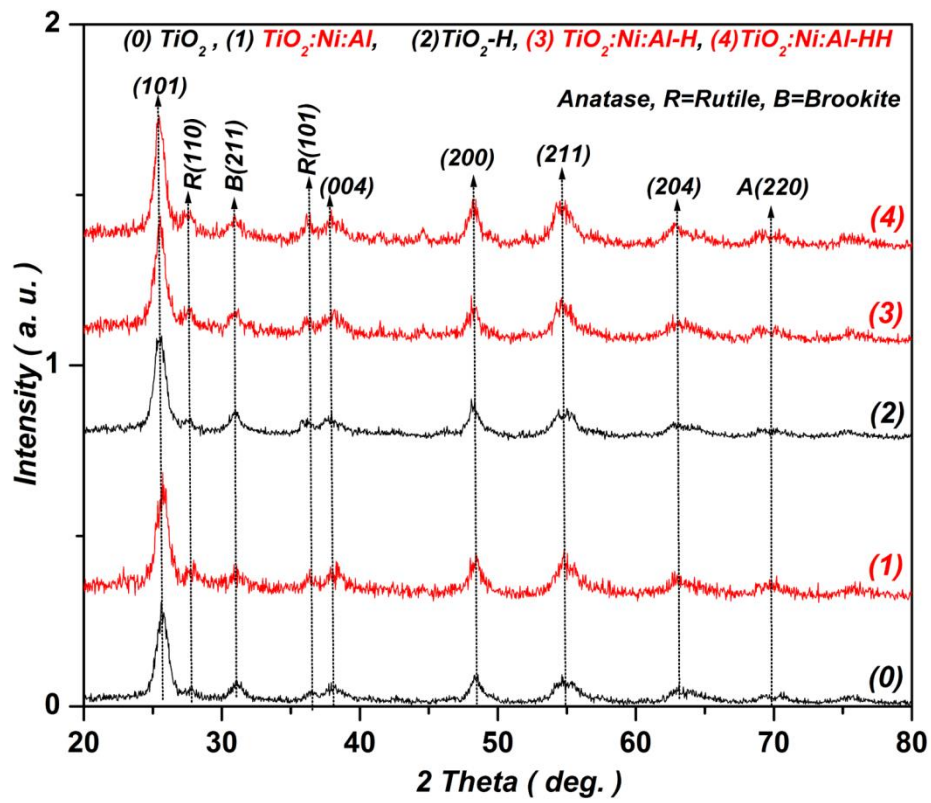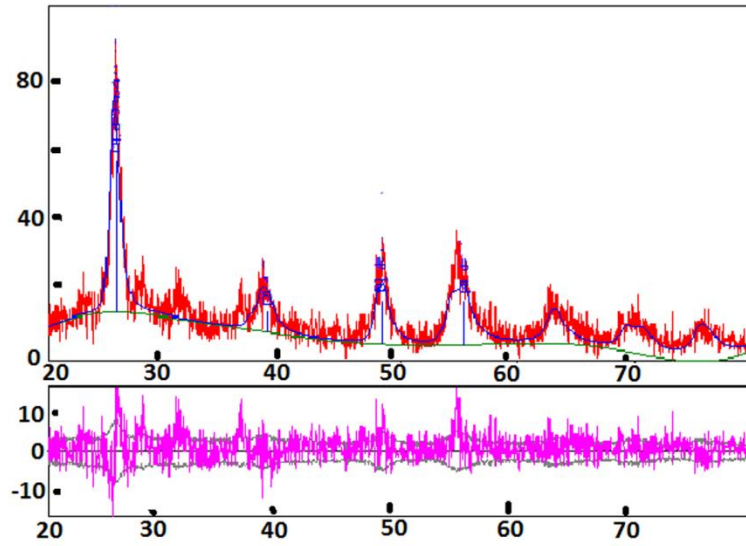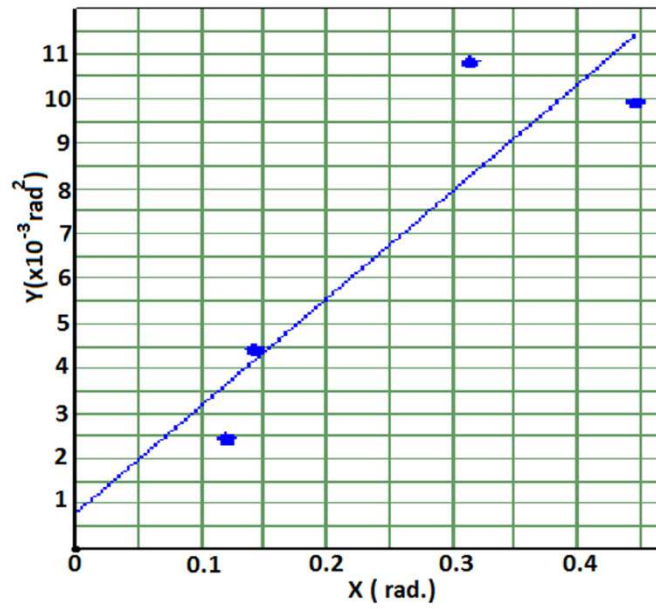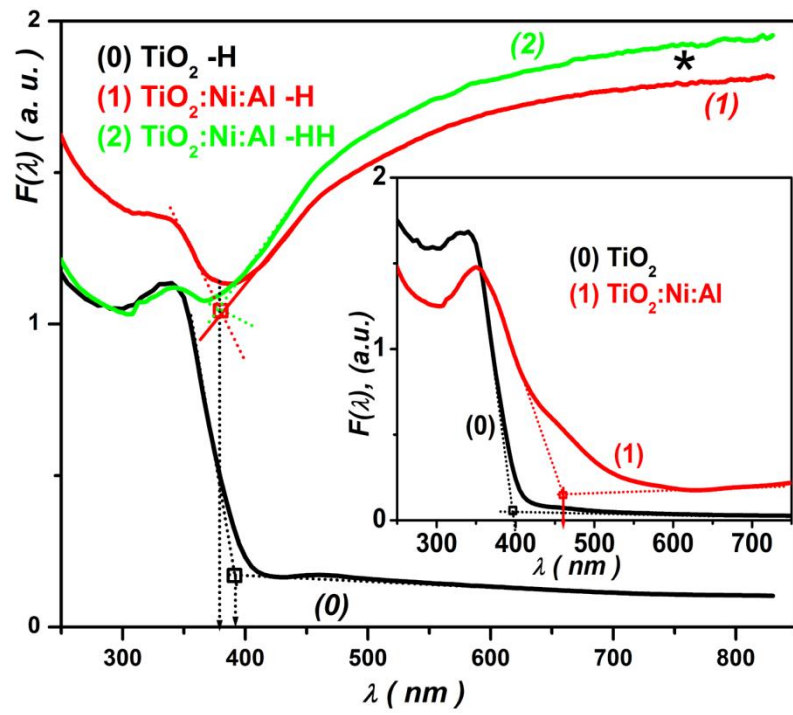
Fig.1a

Fig.1b

Fig.1c

Fig.2
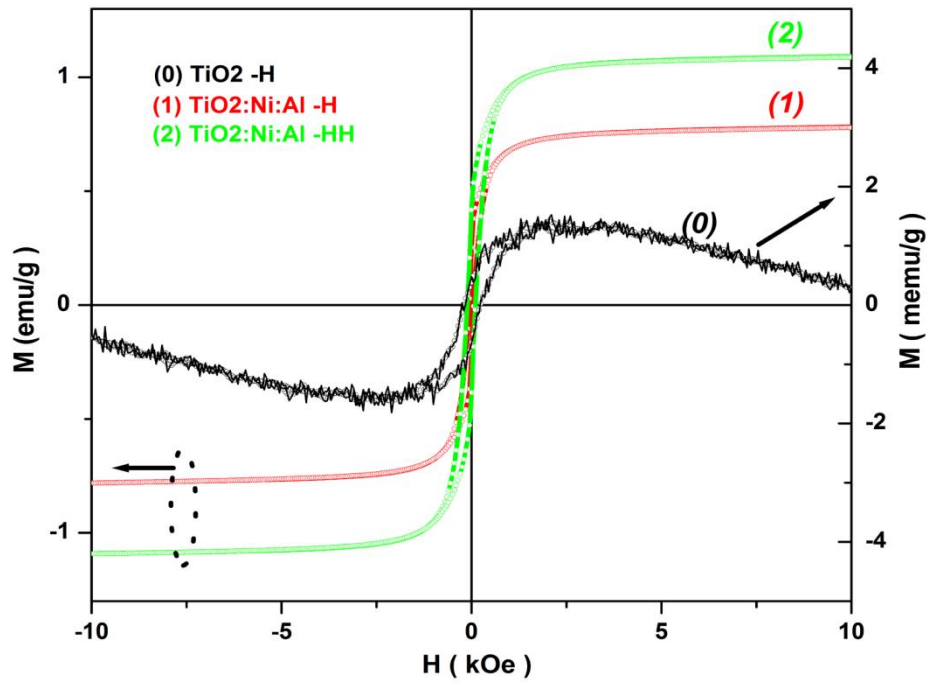
Fig.3

Figures
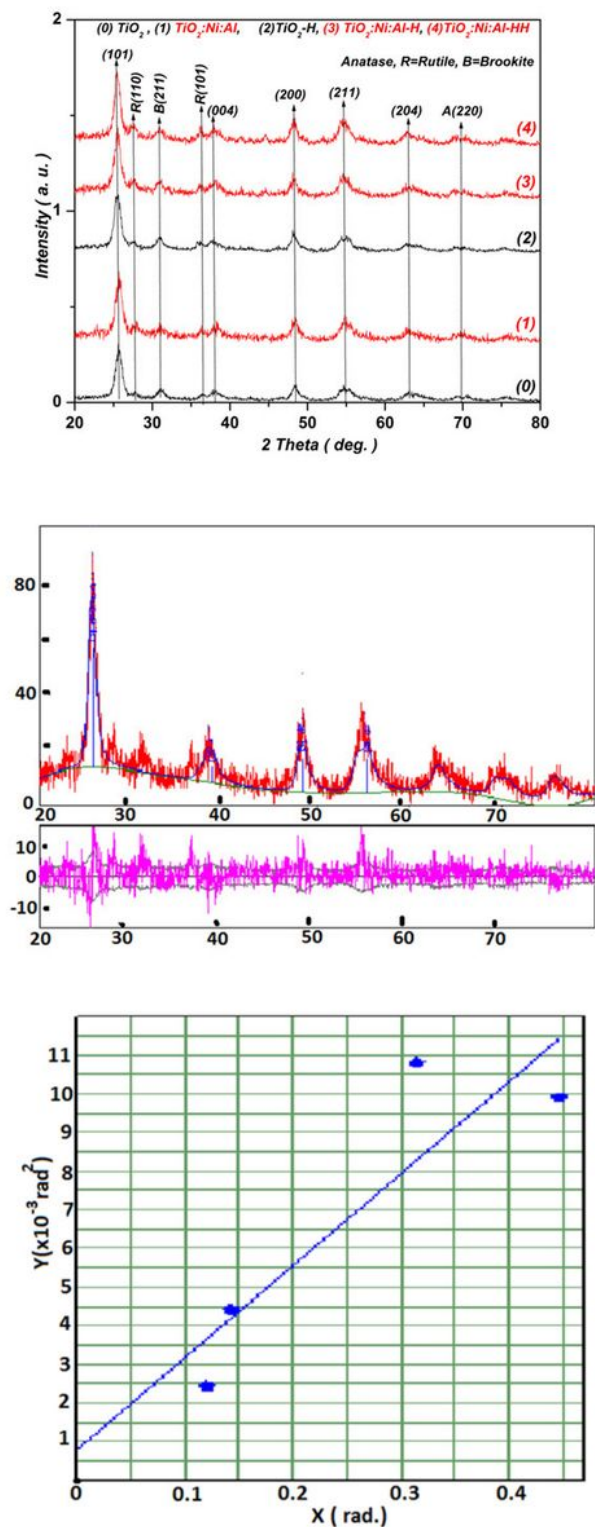
Figure 1

(Top) a: XRD patterns of the synthesized nanopowders; TiO2, TiO2:Ni:Al, TiO2-H, TiO2:Ni:Al-H, and TiO2:Ni:Al-HH. Anatase is the major phase crystallised. (Middle) b: Graphical representation of the Rietveld refinements for TiO2:Ni:Al sample, where; the red solid line (up) is the experimental data, the blue

solid line (up) is the calculated pattern, and the solid pink line (down) is the intensity difference between the calculated and registered. (Bottom) c: H-W plot for TiO2:Ni:Al sample
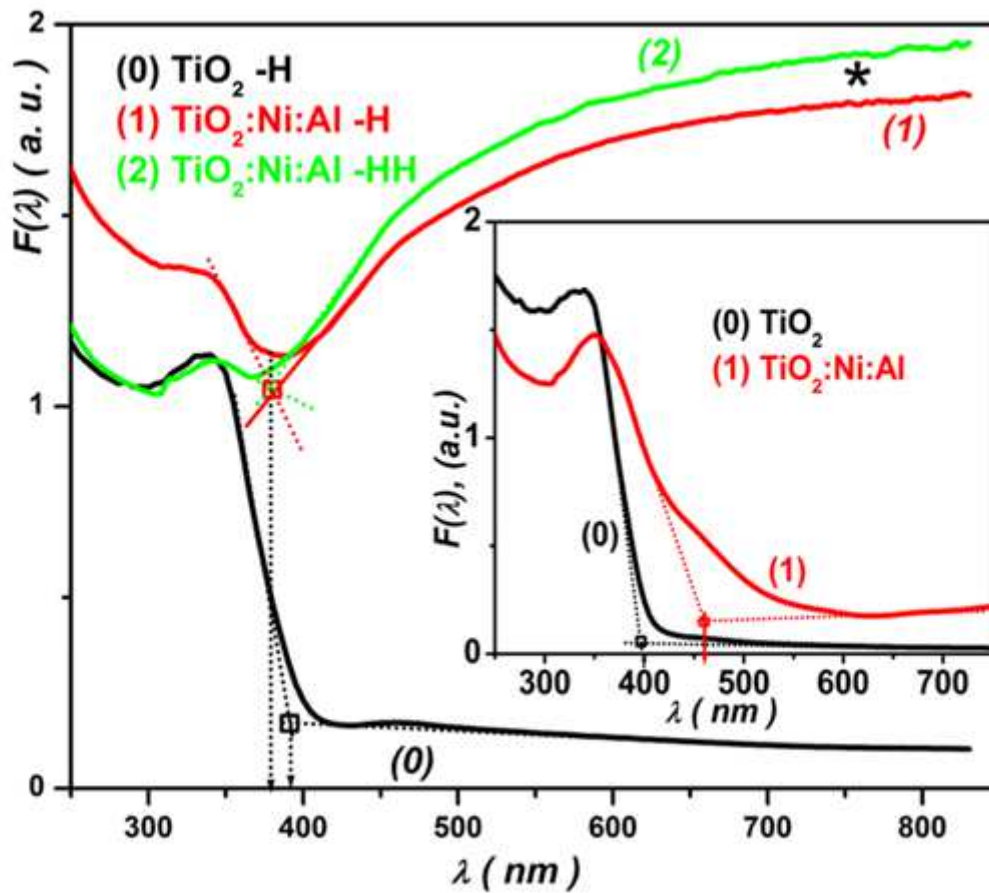

Figure 2

Spectral K-M absorption function; F(λ) of the hydrogenated samples. The thresholds of absorption are shown. The inset shows is the function absorption function F(λ) of the synthesized samples (TiO2 and TiO2:Ni:Al)
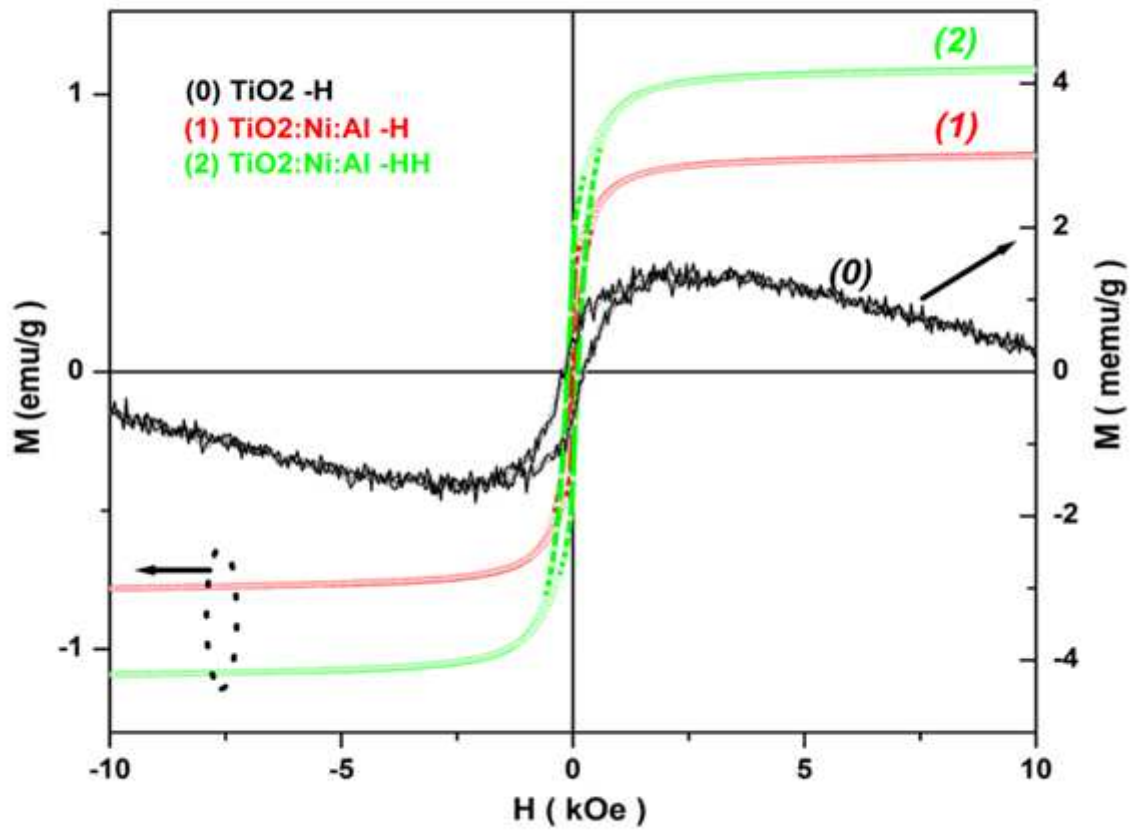
Figure 3

M(H) relationship for the hydrogenated samples.